Defective cortex glia plasma membrane structure underlies light-induced epilepsy in *cpes* mutants

Govind Kunduri[a], Daniel Turner-Evans[b], Yutaka Konya[c], Yoshihiro Izumi[c], Kunio Nagashima[d], Stephen Lockett[e], Joost Holthuis[f], Takeshi Bamba[c], Usha Acharya[g], and Jairaj K. Acharya[a,1]

[a]Cancer and Developmental Biology Laboratory, National Cancer Institute, Frederick, MD 21702; [b]Janelia Research Campus, Howard Hughes Medical Institute, Ashburn, VA 20147; [c]Department of Metabolomics, Kyushu University, Fukuoka 812-8582, Japan; [d]Electron Microscopy Laboratory, National Cancer Institute, Frederick, MD 21702; [e]Optical Microscopy and Analysis Laboratory, Frederick National Laboratory for Cancer Research, Frederick, MD 21702; [f]Molecular Cell Biology Division, University of Osnabrück, 49074 Osnabrück, Germany; and [g]Department of Molecular, Cell and Cancer Biology, University of Massachusetts Medical School, Worcester, MA 01605

Edited by Charles Zuker, Howard Hughes Medical Institute and Columbia University, New York, NY, and approved August 13, 2018 (received for review May 16, 2018)

Seizures induced by visual stimulation (photosensitive epilepsy; PSE) represent a common type of epilepsy in humans, but the molecular mechanisms and genetic drivers underlying PSE remain unknown, and no good genetic animal models have been identified as yet. Here, we show an animal model of PSE, in *Drosophila*, owing to defective cortex glia. The cortex glial membranes are severely compromised in ceramide phosphoethanolamine synthase (*cpes*)-null mutants and fail to encapsulate the neuronal cell bodies in the *Drosophila* neuronal cortex. Expression of human sphingomyelin synthase 1, which synthesizes the closely related ceramide phosphocholine (sphingomyelin), rescues the cortex glial abnormalities and PSE, underscoring the evolutionarily conserved role of these lipids in glial membranes. Further, we show the compromise in plasma membrane structure that underlies the glial cell membrane collapse in *cpes* mutants and leads to the PSE phenotype.

photosensitive epilepsy | sphingolipids | *Drosophila* | neuron | glia

Hypersensitivity and hyperexcitability of neurons lead to spontaneous seizures in epilepsy (1). Photosensitivity is the hallmark of photosensitive epilepsy (PSE) in which seizures are induced upon visual stimulation (2). These stimuli include high-flicker, high-contrast, and high-luminance imagery encountered in daily life (e.g., watching television, playing video games, or attending discotheques), and such photosensitivity is associated with various epilepsy syndromes (3–5). However, the precise mechanisms that underlie the pathophysiology of photosensitive epilepsy are still not clearly understood (2). This could be due in part to the paucity of animal models and the lack of experimental paradigms for evaluating risk factors and the pathological basis for photosensitive epilepsy in human subjects (6).

The behavior of *Drosophila* is coordinated by a network of neuronal circuits that, as in the vertebrate system, comprise the CNS and peripheral nervous system. As in vertebrates, the nervous system is comprised of neural and glial cells, although, there are fewer glial cells than neurons in *Drosophila* (7). The glial cells form a dense network around the neurons and exist in a complex anatomically and physiologically codependent state with them. The cortical region of the *Drosophila* CNS is populated by a single glial subtype known as "cortex glia" that proliferate during the larval stage. In the adult brain, cortex glia encapsulate neuronal cell bodies and neuronal processes that cross through the cortical region before they enter the neuropile (7–9).

Here, we show that ceramide phosphoethanolamine synthase (CPES) is required for the development of cortex glia. In *cpes* mutants, the cortical glia fail to encapsulate the neuronal cell bodies and predispose the flies to photosensitive epilepsy. We show that ceramide phosphoethanolamine (CPE) has a structural role in cortex glial plasma membranes and that the structural analog sphingomyelin (SM) can functionally replace CPE in cortex glial membranes. This study demonstrates a photosensitive epilepsy phenotype in *Drosophila* and shows the importance of cortex glia in this phenotype.

Results

***cpes* Mutants Display Photosensitive Epilepsy.** CPES (CG4585) has been shown to be a bulk CPE-producing enzyme in *Drosophila* (10). We generated CG4585-null flies (*cpes*) using ends-out homologous recombination (Fig. 1*A*). Mass spectrometric analysis of sphingolipids showed about a 95% reduction in CPE levels, suggesting that CG4585 is indeed a bulk CPE-producing enzyme in vivo (Fig. 1*B*). No notable changes were observed in ceramides and hexosylceramides (Fig. 1 *C* and *D* and Dataset S1). Development and survival analysis revealed that about 60–70% of mutants die during the pupal stage or during or immediately after eclosion (Fig. 1*E*). About 25% of mutant flies survive as adults (Fig. 1*E*). Further, about 60% of the *cpes* flies that eclose show a dorsal closure defect (Fig. 1 *G* and *H*). All mutant males are sterile. Immunofluorescence imaging revealed an accumulation of germ cells and a lack of mature sperms (Fig. 1*I*). Ubiquitous expression of UAS CPES completely rescued pupal death, dorsal closure defect, and male sterility phenotypes (Fig. 1 *E* and *G–I*). Longevity analysis showed that *cpes* flies have a significantly reduced life span compared with controls and that this trend is

Significance

Approximately 1 in 100 people have epilepsy, and nearly 3% of epileptics have photosensitive epilepsy, which results in serious debilitating seizures. Despite these numbers, in 100 y of research, no clear single gene defect has been shown to be causative in photosensitive epilepsy in genetic models. Although sphingolipid defects have been shown to be causative for many lysosomal storage diseases in humans as well as animal models, our study shows an important connection to a neuronal disease, photosensitive epilepsy, using the fly system as a model. We show that in a *Drosophila* ceramide phosphoethanolamine synthase-null mutant cortical glial cells fail to establish plasma membrane processes required to encapsulate neuronal cell bodies, resulting in photosensitive epilepsy.

Author contributions: G.K., D.T.-E., Y.K., Y.I., T.B., U.A., and J.K.A. designed research; G.K., D.T.-E., Y.K., Y.I., K.N., T.B., U.A., and J.K.A. performed research; G.K., J.H., U.A., and J.K.A. contributed new reagents/analytic tools; G.K., D.T.-E., Y.K., Y.I., S.L., T.B., U.A., and J.K.A. analyzed data; and G.K., D.T.-E., U.A., and J.K.A. wrote the paper.

The authors declare no conflict of interest.

This article is a PNAS Direct Submission.

[1]To whom correspondence should be addressed. Email: acharyaj@mail.nih.gov.

This article contains supporting information online at www.pnas.org/lookup/suppl/doi:10.1073/pnas.1808463115/-/DCSupplemental.

Published online September 5, 2018.

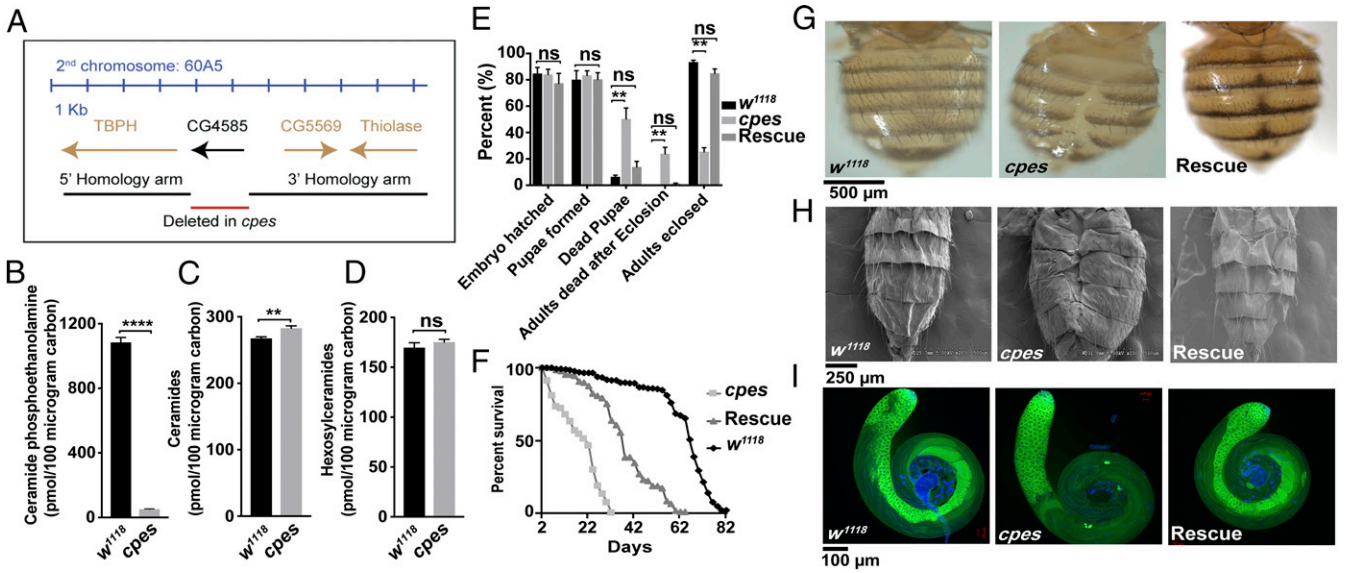

Fig. 1. Generation of *cpes*-knockout flies, sphingolipid analysis, and phenotypes of *cpes* mutants. (*A*) Ends-out homologous recombination was employed to delete CG4585. Coding sequences upstream and downstream of the CG4585 gene are shown by arrows. The homology arms (about 4.6 kb upstream and 3.8 kb downstream) used to target CPES gene are shown as black bars. (*B–D*) CPE (*B*), ceramide (*C*), and monohexosylceramide (*D*) levels in w^{1118} and *cpes* mutants were determined by LC-MS/MS and are expressed as picomoles per 100 µg of total carbon analyzed. Lipids extracted from whole flies were used for analysis. $^{**}P \leq 0.01$; $^{****}P \leq 0.0001$; ns, no significant difference ($P > 0.05$). (*E*) Development and survival of *cpes* mutants. Larvae hatched from the embryos, pupae formed from first-instar larvae, dead pupae, eclosed adults, and adults dead after eclosion were counted manually and expressed as percent. About 300 embryos or larvae were taken for each experiment, and the experiment was repeated twice. $^{**}P \leq 0.01$; ns, $P > 0.05$. (*F*) Longevity analysis of *cpes* mutants ($n = 100$ per experiment, repeated twice). Control flies lived up to 82 d, whereas *cpes* mutants were dead by age 30 d. Overexpression of CPES reversed this trend. (*G* and *H*) Images taken under a light microscope (*G*) and a scanning electron microscope (*H*) show *cpes* mutants have defective dorsal closure (*Center*) compared with control (*Left*); ubiquitous expression of UAS CPES using actin Gal4 completely rescues this defect (*Right*). (*I*) *cpes* mutants are male sterile. Immunostaining of control (*Left*), *cpes* mutant (*Middle*), and CPES rescue (*Right*) testis with anti-vasa protein antibody (green) showed increased accumulation of spermatocytes in *cpes* mutants. Nuclear staining with DAPI (blue) showed the absence of mature sperms in *cpes* mutants. The male sterility phenotype was completely rescued when UAS CPES was expressed ubiquitously.

partially reversed when UAS-CPES is overexpressed ubiquitously (Fig. 1*F*). The partial rescue of longevity has not been probed further and could be due to the driver and/or genetic background.

In addition, we discovered that the *cpes* flies are sensitive to fluctuations in light intensity, and about 70–90% of flies display robust seizures and paralysis when shifted from the dark to ambient light conditions [*SI Appendix*, Movie S1 (w^{1118}), and Movie S2 (*cpes*)]. Upon visual stimulation, the *cpes* mutants displayed classic signs of epilepsy such as seizures, paralysis, tonic–clonic-like activity, recovery seizures, refractory recovery, and complete recovery (Movie S2) (11). The initial seizures and paralysis can be observed within 5–20 s after exposure to ambient light, and complete recovery occurs within 3–4 min even in the presence of continuous light. A minimum of 15-min dark adaptation is required to trigger seizures again. The phenotype manifests fully at day 10 and thereafter. This photosensitivity was fully rescued when CPES was overexpressed ubiquitously (Movie S3).

Visual stimulation is known to trigger seizures and paralysis in human patients with PSE (2). To confirm that this phenotype is indeed due to stimulation through vision, we first recombined $ninaE^{I17}$ (the rhodopsin 1-null mutant) with *cpes* mutants. The major rhodopsin, rhodopsin 1 (Rh1), is expressed in the R1–R6 photoreceptor neurons and therefore causes a significant reduction in vision. Interestingly, the *cpes;* $ninaE^{I17}$ double mutants were still sensitive to light, and PSE was not rescued (Movie S4). This could be due to photoreception through photoreceptor neurons R7 and R8, which express four different types of rhodopsins, Rh3, Rh4, Rh5, and Rh6. The photoreceptor neurons in the ocelli that express Rh2 might also contribute to the photosensitivity in *cpes;* $ninaE^{I17}$ double mutants. Earlier studies have demonstrated that phospholipase C, the enzyme that mediates the hydrolysis of phosphatidylinositol 4,5-bisphosphate [PtdIns(4,5)P_2] to inositol-1,4,5-triphosphate [Ins(1,4,5)P_3] and diacylglycerol, is critical for phototransduction in all photoreceptor neurons, and therefore phospholipase C-null mutants ($norpA^{p24}$) are completely blind (12). Hence, we recombined *cpes* with $norpA^{p24}$. As shown in Movie S4, $norpA^{p24}$; *cpes* double mutants were insensitive to light and rescued the PSE phenotype. The photosensitivity phenotypes of w^{1118}, *cpes*, rescue, *cpes;* $ninaE^{I17}$, and $norpA^{p24}$*; cpes* flies were quantified and averaged for 100 flies as shown in Fig. 2*A*. These experiments demonstrate that the epileptic phenotype displayed by *cpes* flies is a photic response and involves the phototransduction machinery.

Neuronal Activity Is Significantly Increased After Seizure Episodes. Increased neuronal activity is a hallmark of epilepsy. To assess neuronal activity during PSE, we used two-photon calcium imaging from head-fixed *Drosophila* walking freely on an air-suspended ball (Fig. 2*B*; also see *SI Appendix*, *Detailed Materials and Methods*) (13). Intracellular calcium changes have been traditionally used as a proxy for neuronal activity (14). We therefore expressed the calcium sensor UAS-GCaMP6F in all neurons using a pan-neuronal Gal4 driver line (nSyb-Gal4) (15). We then imaged control, *cpes*, and rescued flies before, immediately after, and a few minutes after exposing them to a strobe stimulus of 470-nm light at 1 Hz for 1 min (50% duty cycle, 17 mW/cm^2). For each fly, the imaging volume was centered on the protocerebral bridge, as shown in Fig. 2*C*, to guarantee that the same brain regions were imaged across flies. During the initial recordings, when the fly was in darkness, the pan-neuronal calcium activity fluctuated, often in conjunction with the fly's movements (Fig. 2 *D*, 1–*3*). These fluctuations were observed in the control and rescue flies across all conditions and in the *cpes*

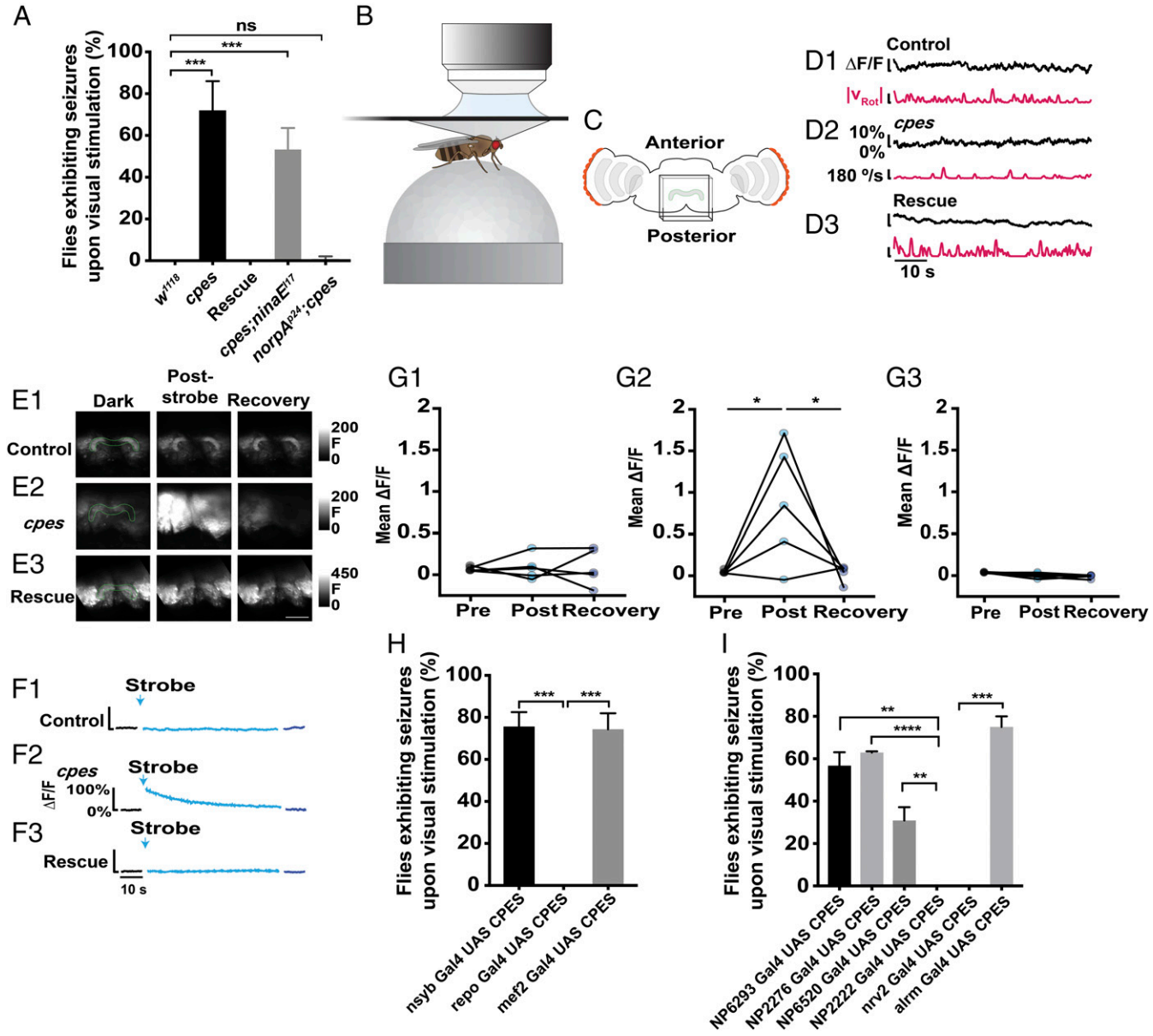

Fig. 2. Analysis of PSE in *cpes* mutants. (*A*) Flies displaying seizures upon visual stimulation were counted manually and are shown as percentages of total fly numbers. Quantification is shown for w^{1118} and *cpes* mutants, CPES rescue (w^-; Actin-Gal4, *cpes/cpes*; UAS-CPES/TM6b), *cpes;ninaE*^{17} double mutants, and *norpA*^{P24}*;cpes* double mutants. About 100 flies were analyzed for each genotype. (*B–H*) Two-photon calcium imaging. (*B*) Schematic of the imaging setup. Flies were allowed to walk freely on the ball while Ca^{2+} activity and the ball position were recorded. (*C*) Overview of the imaged volume. For each fly, the protocerebral bridge was centered in the volume, which consisted of 10 164 × 164 μm planes spaced 8 μm apart. (*D–E*) Multiple 1-min-long baseline trials were recorded in the dark. The fly was then illuminated with 470-nm light at 17 mW/cm^2, 60 Hz, and a 50% duty cycle for 1 min to trigger a seizure. Then 1-min recordings in the dark were performed again. Change in fluorescence intensity normalized to baseline fluorescence intensity was depicted as ΔF/F. (*D*) Examples of Ca^{2+} activity across the volume (black trace) and the fly's rotational speed (pink trace) during prestrobe conditions for a control fly (w^-; *cpes*, UAS-GCaMP6F/CyO; nSyb-Gal4/TM6b or *mkrs*) (*D1*), a *cpes* mutant (w^-; *cpes*, UAS-GCaMP6F/*cpes*; nSyb-Gal4/TM6b or *mkrs*) (*D2*), and a rescue fly (w^-; *cpes*, UAS-GCaMP6F/*cpes*; nSyb-Gal4/CG4585-V5tag) (*D3*). (*E*) Maximum intensity projections of a volume over an entire trial for control (*E1*), *cpes* (*E2*), and rescue (*E3*) flies. The *cpes* fly shows a marked increase in Ca^{2+} after the strobe. (Scale bar: 50 μm.) (*F*) The mean ΔF/F across the entire volume over time during prestrobe (black trace), immediately after the strobe (light blue trace), and after the fly had recovered (dark blue trace) for control (*F1*), *cpes* (*F2*), and rescue (*F3*) flies. (*G*) Mean ΔF/F across the entire volume was averaged over the entire 1-min trial for control (*G1*), *cpes* (*G2*), and rescue (*G3*) flies. Increased Ca^{2+} levels were observed in all *cpes* flies after the strobe, but one fly recovered before the recording session began. (*H*) Quantification of the PSE phenotype upon CPES expression in neurons (w^-; *cpes/cpes*; nSyb-Gal4/UAS-CPES), glia (w^-; *cpes/cpes*; repo-Gal4/UAS-CPES), and muscle tissue (w^-; *cpes/cpes*; mef2-Gal4/UAS-CPES). (*I*) Use of glial subpopulation-specific Gal4 drivers to rescue the PSE phenotype with a UAS-CPES transgene in perineurial glia (w^-; NP6293-Gal4, *cpes/cpes*; UAS-CPES/TM6b or *mkrs*), subperineurial glia (w^-; NP2276-Gal4, *cpes/cpes*; UAS-CPES/TM6b or *mkrs*), ensheathing glia (w^-; NP6520-Gal4, *cpes/cpes*; UAS-CPES/TM6b or *mkrs*), cortex glia (w^-; NP2222-Gal4, *cpes/cpes*; UAS-CPES/TM6b or *mkrs*) (w^-; *cpes/cpes*; UAS-CPES/nrv2-Gal4), and astrocyte-like glia (w^-; *cpes/cpes*; alrm-Gal4/UAS-CPES). About 100 animals per phenotype were analyzed. *$P \le 0.05$; **$P \le 0.01$; ***$P \le 0.001$; ****$P \le 0.0001$; ns, $P > 0.05$; unpaired *t* test.

flies during the recovery period. However, upon visual stimulation with strobed 470-nm light (Movie S5), all *cpes* mutants displayed seizures, in contrast to the control and rescue flies. Further, the *cpes* mutants showed high levels of calcium throughout the brain immediately after the seizure period, which then returned to baseline when the flies recovered from the seizure (Fig. 2 *E*, 2; *F*,

2; and *G*, 2). The control and rescues flies exhibited no such increase (Fig. 2 *E*–*G*).

Abnormal Cortex Glia Are Responsible for Photosensitive Epilepsy. Induction of PSE would minimally involve photoreception followed by widespread neuronal activity that triggers uncontrolled muscular contractions. To determine the tissue or cells responsible for PSE, we used the UAS/Gal4 system to perform tissue-specific rescue experiments in *cpes* mutants. We first tested pan-neuronal, pan-glial, and muscle-specific Gal4 drivers for rescue of photosensitive epilepsy. We found that expression of UAS-CPES with a pan-glial driver, repo-Gal4, completely rescued the PSE phenotype (Fig. 2*H* and Movie S6). Pan-neuronal expression with nSyb-Gal4 and muscle-specific expression with mef2-Gal4 did not rescue the PSE (Fig. 2*H* and Movie S6). This indicates that CPES is required in the glia (and not in neurons or muscles) to regulate seizures induced by visual stimulation.

An adult *Drosophila* brain contains five major glial subtypes: perineurial, subperineurial, cortex, ensheathing, and astrocyte-like glia (7, 8). To probe if aberration in a glial cell subtype was responsible for the PSE phenotype of the mutant, we performed glial subtype-specific rescue with CPES using the UAS/Gal4 system (Fig. 2*I*). We found that expression of UAS-CPES in cortex glia using NP2222-Gal4 fully rescued the PSE phenotype (Fig. 2*I* and Movie S7). Similar results were obtained when CPES was expressed in the cortex glia using a second driver, nrv2-Gal4 (Fig. 2*I* and Movie S7). Recently, a genome-wide RNAi screen identified that de novo sphingolipid biosynthesis, particularly CPE, is crucial for axonal ensheathment of glia in peripheral nerves (16). A partial rescue was observed with an ensheathing glial driver, NP6520-Gal4 (Fig. 2*I* and Movie S7). However, this partial rescue could be due to the expression of NP6520-Gal4 weakly in cortex glia, apart from its strong expression in the ensheathing glia (8). Further, we also noticed expression of markers in some cortex glial cells of *cpes* mutants when driven by NP6520-Gal4 (*SI Appendix*, Fig. S1 *F*, 1 and 2). Perineurial (NP6293-Gal4), subperineurial (NP2276-Gal4), and astrocyte-like (alrm-Gal4) glial-specific expression of CPES did not rescue the PSE phenotype (Fig. 2*I* and Movie S8).

Neuronal Cell Body Encapsulation by Cortex Glia Is Compromised in *cpes* Mutants. Cortex glia are a morphologically distinct cell type that encapsulate individual neuronal cell bodies (7, 8) and provide trophic support to cortical neurons (17). A single cortex glial cell could extend its plasma membranes to encapsulate as few as 22 or as many as 74 neuronal cell bodies through competitive interaction with neighboring cells, forming a highly lamellated honeycomb-like network of membranes in the adult brain (18).

To examine glial cells, we first expressed a plasma membrane-specific protein, UAS-PLCδ-PH-EGFP, by using the pan-glial–specific driver repo-Gal4. We found that, unlike in controls, cortex glia in *cpes* mutants failed to establish a honeycomb-like network around the neuronal cell bodies (DAPI staining shows neuronal cell nuclei) in the cortical region of the midbrain (Fig. 3 *A*, 1 and *B*, 1). Cortex glia in the optic lobes are also similarly affected, and only a few normal-looking cortex glial cells were observed (Fig. 3 *A*, 2 and *B*, 2). The cortical glial phenotype was fully penetrant in the *cpes*-mutant flies and was fully rescued by expression of CPES in glial cells (Fig. 3 *C*, 1 and *2*). Transmission electron microscopy (TEM) analysis of adult brains revealed that in w^{1118} brains the individual neurons are separated by a thin sheet of cortex glial processes (Fig. 3 *D*, 1 and 2). Generally, this sheet showed the presence of four bilayer membranes (Fig. 3 *D*, 3); the two outer membranes correspond to the neuronal plasma membrane, and the two inner membranes were from the cortex glial processes. In the *cpes* mutant, these cortex glial processes were absent (Fig. 3 *E*, 1 and 2). Therefore, at higher magnification (Fig. 3 *E*, *3*) we see only two plasma membranes that correspond to the plasma membrane of neuronal cell bodies, confirming the neuronal cell body encapsulation defect in *cpes* mutants (Fig. 3*E*). This defect was rescued by CPES expression in cortical glial cells (Fig. 3 *F*, 1–3). It is worth noting here that the $norpA^{p24}$ mutant, which is a mutant of phospholipase C, does not exhibit structural abnormalities in the cortical glia, and that the $norpA^{p24}$;*cpes* double mutants still display cortical glial defects (*SI Appendix*, Fig. S2). Thus, the absence of light-induced epilepsy in $norpA^{p24}$;*cpes* double mutants is due solely to blindness and not to rescue of the glial phenotype.

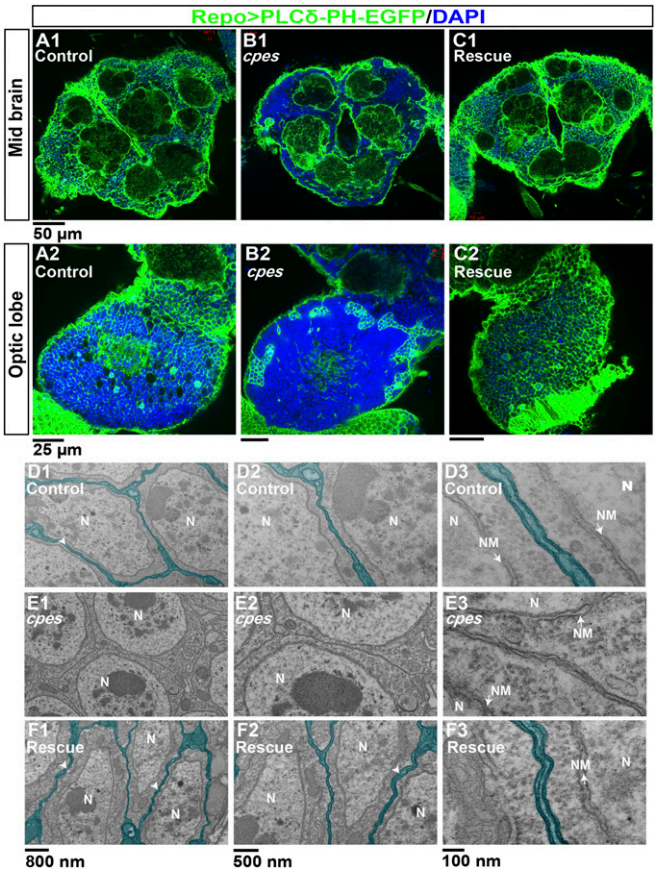

Fig. 3. Cortex glia are compromised in *cpes* mutants. (*A*–*C*) UAS-PLCδ-PH-EGFP was driven by the pan-glial driver repo-Gal4 in all genotypes. Brains were dissected and immunostained with anti-GFP antibody, and immunofluorescence imaging was performed using confocal microscopy. (*A1*) Control midbrain. (*A2*) Control optic lobe. (*B1*) *cpes* midbrain. (*B2*) *cpes* optic lobe. (*C1*) CPES rescue midbrain. (*C2*) CPES rescue optic lobe. (*D*–*F*) Ultrastructural analysis of cortex glia in adult fly brains. (*D1*, *E1*, and *F1*) TEM images for w^{1118} (*D1*), *cpes* (*E1*), and rescue (w^{-}; NP2222-Gal4, *cpes*/*cpes*; UAS-CPES/TM6b or *mkrs*) (*F1*) brains. (*D2* and *D3*, *E2* and *E3*, and *F2* and *F3*) Higher-magnification images of a selected area in w^{1118} (*D2* and *D3*), *cpes* (*E2* and *E3*), and rescue (*F2* and *F3*) brains. Cortex glial membrane processes are shown with false color (light blue green). Occasionally, two overlapping cortex glial processes are observed between neuronal cell bodies (arrowheads). N, neuron nuclei; NM, nuclear membrane (white arrows).

Cortex Glia in *cpes* Mutants Are Compromised Throughout Development. Cortex glia appear as early as embryonic stage 16 wherein they form larger chambers to encapsulate multiple neurons (9). As development proceeds, the cortex glial membranes begin to encapsulate individual neuronal cell bodies, resulting in a honeycomb-like morphology in the adult brain. To determine the fate of cortex glia during earlier stages of development, we expressed membrane RFP (UAS-mCD8-ChRFP) in cortex glia using the nrv2-Gal4 driver, immunostained the embryos, and dissected brains at different

stages of development. As shown in Fig. 4 *A*, 1 and *B*, 1, cortex glial processes in control stage 16 embryo and in first-instar larval brains formed uniform large chambers that encapsulated multiple neurons (consisting of neuroblasts and their lineages whose nuclei are seen stained blue with DAPI). During the second- and third-instar larval stages cortex glia appear as a trophospongium, wherein glia both form large chambers and individually encapsulate neurons in small chambers (Fig. 4 *C*, 1 and *D*, 1). By the end of pupal stage, in control brains, all neurons are individually wrapped and form the honeycomb-like morphology (Fig. 4 *E*, 1 and *F*, 1). In *cpes* mutants, the cortex glia formed aberrant processes that did not establish large chambers and encapsulate the neuronal cell bodies (Fig. 4 *A*, 2 and *B*, 2). The cortex glial processes were malformed in *cpes* mutants even in second- and third-instar larval brains, and neurons lacking cortex glial encapsulation became more evident (Fig. 4 *C*, 2 and *D*, 2). The honeycomb-like morphology was almost completely disrupted in the pupal stage, and only a few normal-looking cells were observed (Fig. 4 *E*, 2 and *F*, 2).

Cortex glia maintain low cell numbers during the early stages of larval development (until the late second-instar stage). However, during the third-instar stage they proliferate extensively. This proliferation correlates with neuronal proliferation, and systemic cues derived from neuronal stem cells remodel the cortex glia (9, 19). To determine whether cortex glial cell number or proliferation was compromised during development, we expressed nuclear-specific RFP (UAS-mCherry.NLS) in cortex

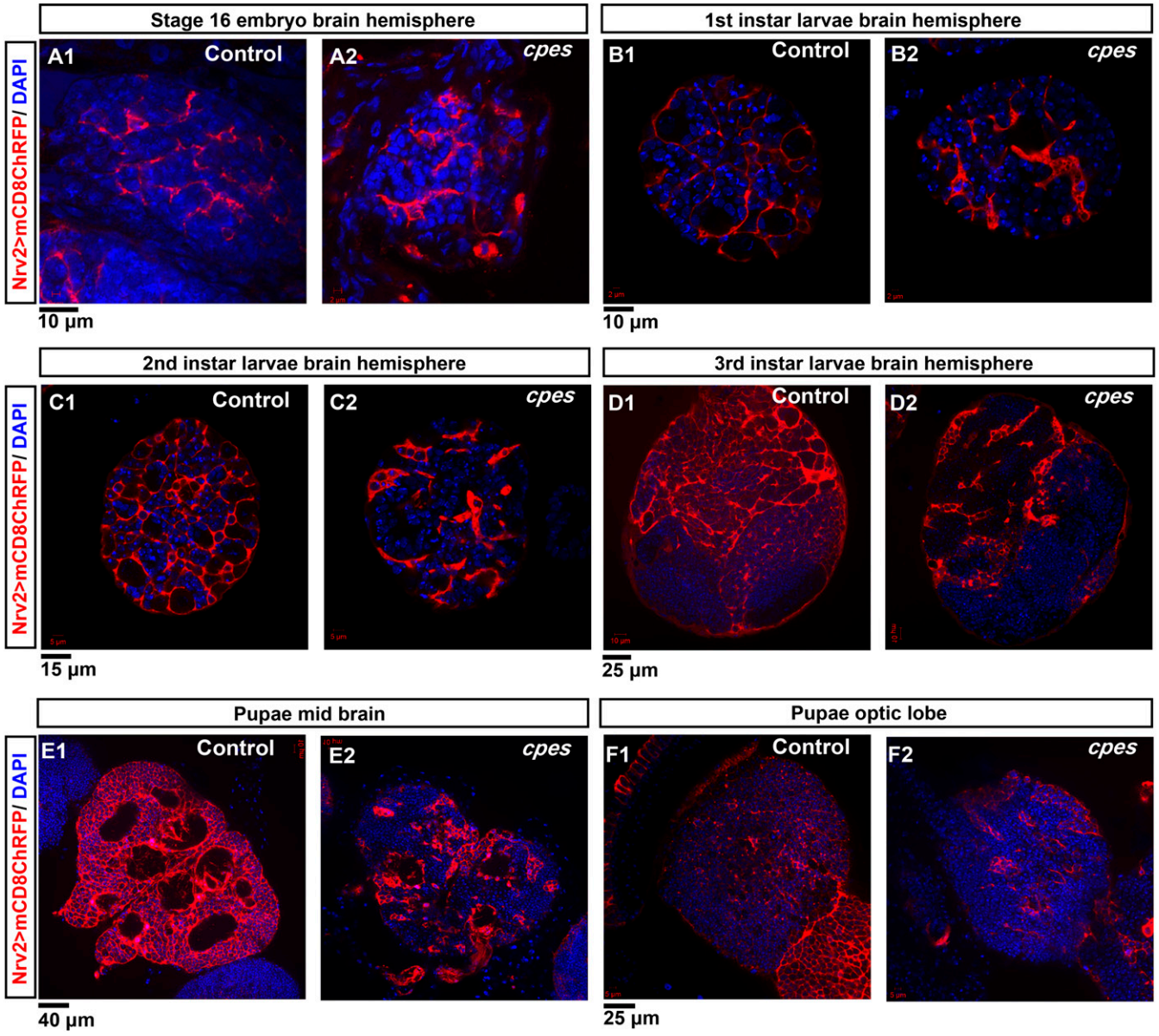

Fig. 4. Cortex glia are compromised throughout development. Membrane-specific UAS-mCD8-ChRFP was expressed in the cortex glia using nrv2-Gal4, and brains at different stages of development were dissected and immunostained with dsRed antibody. The genotype of control flies is w^{-}; *cpes*/Actin-GFP-CyO; nrv2-Gal4, UAS-mCD8-ChRFP/TM6b, and the genotype of *cpes* flies is w^{-}; *cpes*; nrv2-Gal4, UAS-mCD8-ChRFP/TM6b. (*A*) Stage 16 embryo brain hemisphere of a control fly (*A1*) and a *cpes*-mutant fly (*A2*). (*B*) First-instar larval brain hemisphere of a control fly (*B1*) and a *cpes*-mutant fly (*B2*). (*C*) Second-instar larval brain hemisphere of a control fly (*C1*) and a *cpes*-mutant fly (*C2*). (*D*) Third-instar larval brain hemisphere of a control fly (*D1*) and a *cpes*-mutant fly (*D2*). (*E*) Midbrains of a control pupa (36–48 h post pupation) (*E1*) and a *cpes*-mutant pupa (*E2*). (*F*) Optic lobes of a control pupa (*F1*) and a *cpes*-mutant pupa (*F2*). The nrv2-Gal4 expression is weak in pupal optic lobes (36–48 h post pupation).

glia using NP2222-Gal4. We found that the number of cortex glia did not change significantly between control and mutants during the first-instar larval stage (*SI Appendix*, Fig. S3 *A–D*). However, *cpes* mutants showed reduced numbers of cortex glia in second-instar and a moderate reduction in third-instar and adult brains (*SI Appendix*, Fig. S3 *E–P*), indicating that CPES is required to establish the full complement of cortical glial cells. These findings suggest that in *cpes* mutants the cortex glia fail to establish consistent membrane processes that can fully encapsulate neuronal cell bodies, thereby disrupting its relationship with neurons.

SM Can Functionally Replace CPE in Cortex Glial Membranes. *Drosophila* lack SM, which is found in mammalian membranes. Instead, they synthesize an SM structural analog, CPE, that differs in its head group (Fig. 5 *A* and *B*) (20). Mammalian cells contain two SM synthase isoforms, SMS1, which is responsible for the bulk production of SM in the *trans* Golgi lumen, and SMS2, which is responsible for regenerating SM from ceramide released by sphingomyelinases at the plasma membrane (21). SMS2 is a bifunctional enzyme with SM synthase and CPE synthase activities, while SMS1 is a largely monofunctional enzyme with SM synthase activity (22). SM and CPE are structurally identical in their tail groups, which are buried in the lipid bilayer, and perhaps are functionally similar in providing structural stability to the plasma membrane and/or stability to membrane proteins. We wondered whether SM could functionally replace the role of CPE in cortex glial membranes. To address this possibility, we generated transgenic flies that expressed V5-tagged human SM

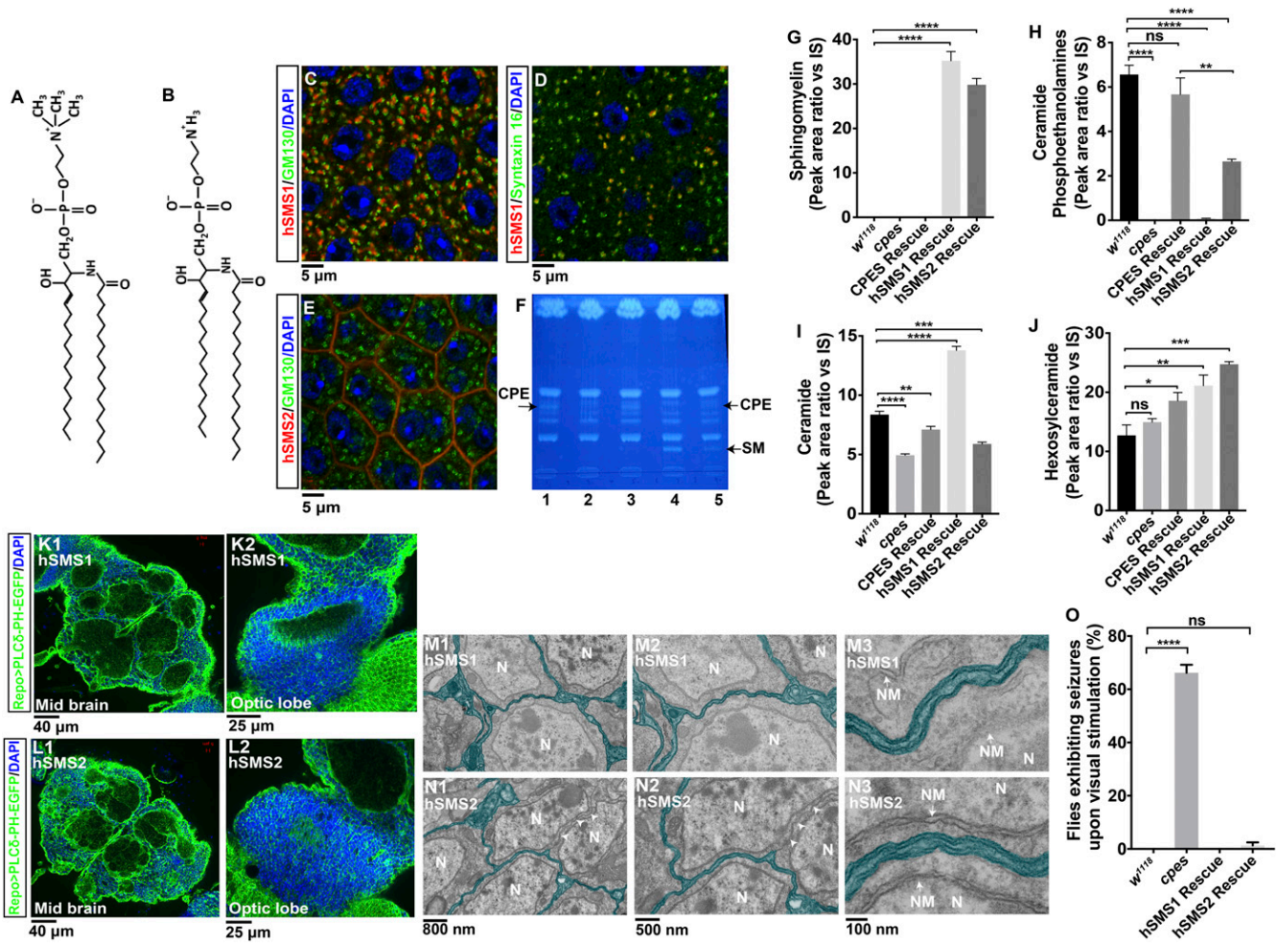

Fig. 5. SM can functionally replace CPE in cortex glial membranes. (*A*) Chemical structure of SM. (*B*) Chemical structure of CPE. (*C*) Localization of hSMS1 in relation to the *cis* Golgi marker GM130 in male collecting ducts; red, hSMS1-V5tag; green, GM130; blue, DNA. (*D*) Colocalization of hSMS1 with the *trans* Golgi marker in male collecting ducts; red, hSMS1-V5tag; green, Syntaxin16; blue, DNA. (*E*) Localization of hSMS2 with the *cis* Golgi marker GM130 in male accessory glands; red, hSMS2-V5tag; green, GM130; and blue, DNA. (*F*) TLC of lipids extracted from 10 fly heads from each genotype: w^{1118} (lane 1), *cpes* (lane 2), CPES rescue (lane 3), hSMS1 rescue (lane 4), and hSMS2 rescue (lane 5). The position of SM and CPE on TLC are indicated with arrows. (*G–J*) Sphingolipid levels in lipid extracts from fly heads were measured by SFC-MS/MS and are expressed as peak area ratio vs. internal standards (IS). All lipid samples were normalized to carbon content. *$P \leq 0.05$; **$P \leq 0.01$; ***$P \leq 0.001$; ****$P \leq 0.0001$; ns, $P > 0.05$; unpaired *t* test. (*K*) UAS-hSMS1-V5tag and UAS-PLCδ-PH-EGFP were expressed using the pan-glial driver repo-Gal4 (w^{-}; *cpes*; repo-Gal4, UAS-PLCδ-PH-EGFP/UAS-hSMS1-V5tag) in midbrain (*K1*) and optic lobe (*K2*). (*L*) UAS-hSMS2-V5tag and UAS-PLCδ-PH-EGFP were expressed using the pan-glial driver repo-Gal4 (*w-*; *cpes*; repo-Gal4, UAS-PLCδ-PH-EGFP/UAS-hSMS2-V5tag) in midbrain (*L1*) and optic lobe (*L2*). (*M* and *N*) Ultrastructural analyses of cortex glia in hSMS1 (*M*) and hSMS2 (*N*) rescued adult brains. (*M1*) TEM image for hSMS1 rescue (w^{-}; *cpes*, Actin Gal4/*cpes*; UAS-hSMS1-V5tag/TM6b or *mkrs*). (*M2* and *M3*) Higher-magnification images of a selected area from *M1*. (*N1*) TEM image for hSMS2 rescue (w^{-}; *cpes*, Actin-Gal4/*cpes*; UAS-hSMS2-V5tag/TM6b or *mkrs*). (*N2* and *N3*) Higher-magnification images of a selected area from *N1*. Cortex glial membrane processes are shown with false color (light blue green). N, neuron nuclei; NM, nuclear membrane (white arrows). Missing cortex glial processes between the neurons are indicated by white arrowheads. (*O*) Quantification of the PSE phenotype upon hSMS1 (w^{-}; *cpes*, Actin Gal4/*cpes*; UAS-hSMS1-V5tag/TM6b or *mkrs*) and hSMS2 (w^{-}; *cpes*, Actin-Gal4/*cpes*; UAS-hSMS2-V5tag/TM6b or *mkrs*) expression. Unpaired *t* test, ****$P < 0.0001$; ns, $P > 0.05$.

synthase 1 (hSMS1) and human SM synthase 2 (hSMS2) under UAS control. Both proteins localized to their respective physiological compartments (we used male accessory glands for immunolocalization due to the prominent Golgi compartments in these cells) (Fig. 5 *C–E*) (23). To determine whether these enzymes catalyze SM synthesis in *Drosophila*, we extracted total lipids from fly heads and analyzed them using TLC. As shown in Fig. 5*F*, lipid extracts from hSMS1 and hSMS2 showed significant amounts of SM (Fig. 5*F*, lanes 4 and 5), and, as expected, SM was not detected in fly extracts from w^{1118}, *cpes*, and CPES rescue samples (Fig. 5*F*, lanes 1–3). The amount of SM made by hSMS1 was significantly higher than the amount made by hSMS2, perhaps due to the lower amount of ceramide present at the plasma membrane compared with the Golgi (Fig. 5*F*, lanes 4 and 5). Interestingly, as previously reported (22, 24), hSMS2 produced both CPE (in small amounts) and SM (Fig. 5*F*, lane 5). Consistently, *cpes* mutants (Fig. 5*F*, lane 2) showed a dramatic reduction in CPE levels that was rescued by overexpression of CPE synthase (Fig. 5*F*, lane 3). Further, we performed supercritical fluid chromatography coupled to mass spectrometry (SFC-MS/MS) to analyze sphingolipids in fly heads (Dataset S2). As shown in Fig. 5*G*, SM was detected only in hSMS1 and hSMS2 rescue flies. The hSMS2 rescue flies also accumulated a significant amount of CPE, but no CPE was detected in *cpes* mutants or hSMS1 rescue flies (Fig. 5*H*). Ceramide is moderately increased in hSMS1 rescue flies (Fig. 5*I*). Hexosylceramides are slightly increased in all CPES, hSMS1, and hSMS2 rescue samples (Fig. 5*J*).

To determine whether hSMS1 could rescue the cortex glial abnormality, we overexpressed UAS-hSMS1 and UAS-PLCδ-PH-EGFP (to label the plasma membrane) in glial cells using repo-Gal4. As shown in Fig. 5 *K*, 1 and 2, expression of hSMS1 completely rescued the cortex glial-encapsulating defects. This result emphasizes the evolutionarily conserved role of SM in glial membranes. The expression of plasma membrane-specific hSMS2 also rescued the cortex glial phenotype (Fig. 5 *L*, 1 and 2), suggesting that the SM/CPE produced locally on the plasma membrane is sufficient to rescue the cortex glial phenotype. TEM analysis further confirmed these results (Fig. 5 *M* and *N*). However, minor defects in encapsulation are apparent in certain areas of hSMS2 rescue brains (white arrowheads in Fig. 5 *N*, 1 and 2). It is worthwhile to note that ubiquitous expression of either hSMS1 or hSMS2 rescued most of the phenotypes of *cpes* mutants including pupal death, dorsal closure defect (*SI Appendix*, Fig. S4), and PSE (Fig. 5*O* and Movie S9). However, both hSMS1 and hSMS2 failed to rescue the male sterility phenotype, suggesting that *Drosophila* CPES might play a unique role in spermatogenesis.

Altered Plasma Membrane Structure Is Responsible for Cortical Neuronal Encapsulation Defects. Similar to SM synthesis in mammals, CPE synthesis in *Drosophila* occurs in the Golgi complex (21). It was shown that inhibition of SM synthesis reduces the rate of secretion of several proteins, particularly GPI-anchored proteins, from the Golgi to the plasma membrane (25–27). To examine the effect of perturbing CPE synthesis on the trafficking of membrane proteins, we transiently expressed UAS-GFP-GPI and UAS-mCD8-ChRFP using hsp70-Gal4. The conditional hsp70-Gal4 does not transcribe at room temperature but can be induced to express maximally at 37 °C (28). After heat shock at 37 °C for 1 h, flies were recovered at 25 °C for 12 or 24 h and were analyzed (*SI Appendix*, Fig. S5 *A–L*). Hsp70-Gal4 is expected to express in all cell types when induced by heat shock. However, we found that the expression of GFP-GPI and mCD8-ChRFP is stronger in glia than in neurons (*SI Appendix*, Fig. S5 *A–L*). Confocal images were taken from the medullary region in the optic lobes, primarily due to the presence of elaborate glial membranes that showed strong expression of membrane proteins upon heat shock. Both GPI-anchored GFP and mCD8-ChRFP were localized to the plasma membrane within 12 h of induction in control and *cpes* mutants (*SI Appendix*, Fig. S5 *A–L*). A similar localization pattern was seen at 24 h after heat shock (*SI Appendix*, Fig. S5 *A–L*). To further confirm membrane localization of these proteins, we isolated plasma membrane from flies 24 h after heat shock using sucrose density gradient centrifugation, and fractions were analyzed by Western blotting. Na^+K^+-ATPase was used as a marker for the plasma membrane. As shown in *SI Appendix*, Fig. S5 *M–P*, both GFP-GPI and mCD8-ChRFP are present in plasma membrane fractions (*SI Appendix*, Fig. S5 *M–P*). The amount of GFP-GPI and mCD8-ChRFP is comparable in control and *cpes* mutants. These results indicate that post-Golgi trafficking of membrane proteins may not be impaired in *cpes* mutants.

SM has been shown to protect plasma membrane lipids from reactive oxygen species (29, 30). Oxidative stress has been shown to cause plasma membrane damage and rapid aging in ceramide transfer protein ($dcert^1$)-null mutants (31). However, this was not a causative factor in the *cpes*-mutant phenotype, since expression of superoxide dismutase and catalase did not rescue the cortex glial morphology (*SI Appendix*, Fig. S6).

We then turned our attention to the plasma membrane, the site of CPE localization and function. The plasma membrane is enriched in phospholipids together with cholesterol and sphingolipids. To determine the status of membrane lipids in *cpes* mutants, we performed in vivo metabolic labeling with ^{32}P-labeled orthophosphoric acid. TLC analysis of lipids extracted from fly heads showed that, compared with controls, *cpes* mutants have high amounts of lysophospholipids, including lysoPC and LysoPE (Fig. 6 *A* and *B*). SM has been shown to negatively regulate phospholipases (cPLA2 and sPLA2) in the plasma membrane (32, 33). We wondered whether the plasma membrane in *cpes* mutants is increasingly damaged due to activation of phospholipases. To confirm these findings, we performed metabolomic profiling of w^{1118} and *cpes* mutants. About 301 metabolites were identified and classified into different functional pathways (Dataset S3). As shown in Fig. 6*C*, lysophospholipids are significantly increased in *cpes* mutants (Dataset S3). These results indicate altered plasma membrane composition and properties. SM/CPE along with glycosphingolipids and cholesterol form specialized liquid-ordered domains commonly referred to as "rafts" or isolated detergent-resistant membranes (DRMs) (20). Several membrane proteins, including transmembrane proteins and GPI-anchored proteins, are shown to be preferentially enriched in DRMs. These membrane domains are resistant to detergent treatment (1% Triton X-100) on ice and float to low density on sucrose or OptiPrep gradients. The DRMs are known to regulate a number of processes involving signal transduction, cell adhesion, membrane sorting, and pathogen entry (34–38). We wanted to determine whether the lack of CPE compromises the DRM in *cpes* mutants and could thus drive all other plasma membrane defects. To assess the DRMs, we extracted the DRMs from fly head samples using standard protocols (39). As shown in Fig. 6*D*, DRMs localize to the low-density fraction of a sucrose gradient and form an opaque white band. Compared with control flies (Fig. 6*D*, lane 1), this DRM band was not visible in *cpes* mutants (Fig. 6*D*, lane 2). The DRM band reappeared when *cpes* mutants were rescued with UAS-CPES (lane 3) or UAS-hSMS1 (lane 4). Further fractions collected from top to bottom of the sucrose gradient were subjected to Western blotting analysis with contactin and anti-HRP antibodies. Contactin is a GPI-anchored protein, and it was previously shown to localize to glial cell septate junctions (40). Western blotting analysis showed that contactin is present in DRM fractions in control flies but is absent in *cpes* mutants (Fig. 6 *E* and *F*). CPES or hSMS1 overexpression rescued the contactin translocation into DRM fractions (Fig. 6 *G* and *H*). Na^+ K^+-ATPase is a non-DRM plasma membrane protein and therefore is present only in the bottom fractions, and it was comparable in

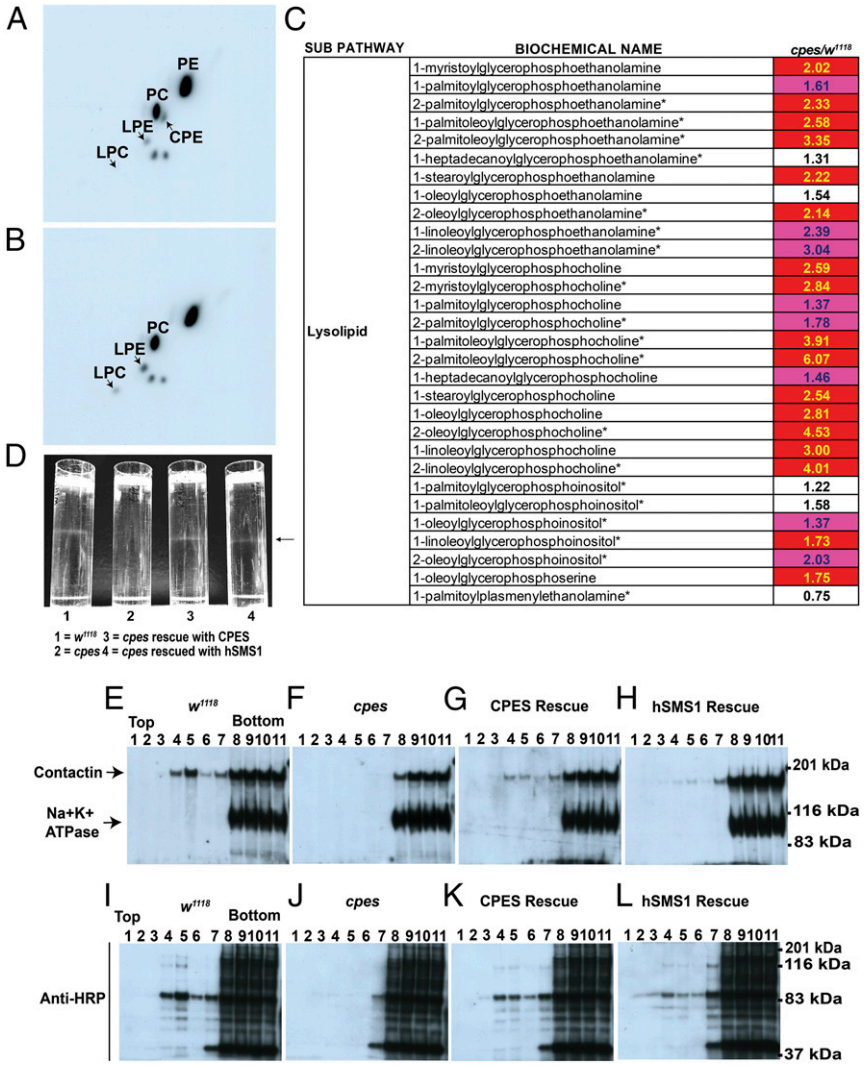

Fig. 6. Plasma membrane structure is compromised in *cpes* mutants. (*A* and *B*) Metabolic labeling of phospholipids and 2D TLC analysis. Newly eclosed flies were grown on regular food containing 50 μCi/mL [^{32}P] orthophosphate for 10 d. (*A*) Phospholipid profile of w^{1118} flies. (*B*) Phospholipid profile of *cpes* flies. Loading was normalized by taking lipid extracts containing an equal number of cpm. The position of lysophospholipids and possible CPE are indicated by arrows. (*C*) Metabolomic analysis. Lysophospholipids are significantly accumulated in *cpes* mutants. Red with gold text indicates significantly ($P \leq 0.05$) high levels in *cpes* mutants compared with w^{1118} mutants (metabolite ratio >1). Magenta with blue text indicates the statistical cutoff for significance was narrowly missed ($0.05 < P < 0.10$). White with black text indicates no statistically significant difference between w^{1118} and *cpes* mutants. (*D–L*) DRMs/rafts are compromised in *cpes* mutants. (*D*) A representative image showing isolated DRMs from fly heads. The arrow indicates the position of the DRM fraction. Column 1, w^{1118}; column 2, *cpes*; column 3, CPES rescue (w^{-}; *cpes*, Actin-Gal4/*cpes*; UAS-CPES/TM6b or *mkrs*); column 4, hSMS1 rescue (*w–*; *cpes*, Actin-Gal4/*cpes*; UAS-hSMS1_V5/TM6b or *mkrs*). (*E–L*) One-milliliter fractions were obtained from the top to the bottom of the sucrose gradient. About 20 μL of each fraction from control (*E* and *I*), *cpes* (*F* and *J*), CPES rescue (*G* and *K*), and hSMS1 rescue (*H* and *L*) samples was loaded per well and analyzed by Western blotting. Immunoblotting was performed with anti-contactin antibody (*E–H*), Na^{+}, K^{+}-ATPase antibody (*E–H*), and anti-HRP antibody (*I–L*). The positions of protein bands are indicated by arrows.

all backgrounds (Fig. 6 *E–H*). Anti-HRP antibody is known to cross-react with several proteins from neuronal tissue containing α1,3-fucosylated N-glycans, which are cell-surface proteins (41). Western blotting with anti-HRP antibody revealed that several HRP cross-reacting proteins are present in the control DRM fractions (Fig. 6*I*), the most apparent one with a mass around 83 kDa. These HRP cross-reacting proteins are significantly lower in DRM fractions of *cpes* mutants (Fig. 6*J*) and are rescued when CPES or hSMS1 is overexpressed ubiquitously (Fig. 6 *K* and *L*). In summary, these results strongly suggest that the failure to establish DRMs due to a lack of CPE leads to the cortex glial encapsulation defect.

Discussion

Visual stimulation of seizures, also known as PSE, is well documented in human patients (2). It is estimated that about 2–14% of epilepsy patients have a chance of developing photic-induced seizures (3, 42). However, the mechanisms responsible for photosensitive epilepsy are not clearly understood (2). Several mutants isolated in *Drosophila* display seizures and paralysis when stimulated mechanically (bang sensitive) and therefore serve as a wonderful model for epilepsy (43). However, light-induced seizures have not been experimentally described in *Drosophila*. In the present study, we demonstrate a photosensitive epilepsy and use this phenotype as a tool to discover the underlying pathology in the *cpes*-mutant brains (Fig. 2). In the mammalian system, neuron and glia interactions are complex, wherein a single mature astrocyte (also embedded within the cell cortex and structurally similar to the cortex glia in *Drosophila*) can wrap multiple neuronal cell bodies (somata), hundreds of dendrites, and thousands of individual synapses (44, 45). This complex interaction of glia with

neurons makes it difficult to study the role of glia selectively at synapses or at the cell body. In *Drosophila*, neuronal cell bodies and neuronal synapses are spatially separated and are supported by cortex and neuropile glia, respectively. This allows us to study neuronal cell body and glial interactions independent of the synapses, which is challenging in the mammalian system (18). Although a number of studies have showed that astrocytes play crucial role in epilepsy in mammals (46), much remains to be investigated, especially the role of aberrant glia and neuronal cell body interactions in epilepsy. The *cpes* mutants described here serve as a powerful model to study the mechanisms responsible for photosensitive epilepsy. The availability of genetic tools and the ease of performing physiology experiments in live animals allow *Drosophila* to serve as a promising model for PSE.

In this study, we have shown that CPES is essential for the encapsulation of neuronal cell bodies by cortex glia. Our study suggests that in *cpes* mutants the plasma membrane fails to establish DRMs and protein fails to segregate into these DRMs. That CPE/SM is enriched in plasma membrane DRMs (microdomains) has been known for a long time (20, 47). Further, a number of studies have shown that blocking SM biosynthetic pathways affects the formation of microdomains and subsequent segregation of membrane proteins into microdomains (48–51). We find that microdomain formation and translocation of membrane proteins, including GPI-anchored proteins, into these microdomains was significantly compromised in the *cpes* mutants (Fig. 6 *D–L*). Expression of hSMS1 that synthesizes SM, a structural analog of CPE, rescued microdomain formation and the translocation of membrane proteins into microdomains (Fig. 6 *D–L*). These data demonstrate that the head group of CPE/SM has no significant role in the formation of microdomains at the plasma membrane. Perturbations in the microdomains compromise plasma membrane structure and function (52). The impact of this deficiency is felt most in circumstances associated with massive membrane expansion, such as elaboration of cortical glial membrane processes.

A seizure is a clinical manifestation of an abnormal, excessive, hypersynchronous discharge of a population of cortical neurons (53). One possible role of cortex glia in seizures is to prevent hypersynchronization of brain neurons by regulating ion balance at the interface between neuronal cell bodies. Consistent with this hypothesis, disruption of the cortex glial-specific Na^+/Ca^{2+}, K^+ exchanger prevented microdomain Ca^{2+} oscillations and increased susceptibility to seizures (54). Other possible roles of cortex glia include (*i*) providing insulation to the neuronal cell bodies, thereby protecting them from electrical crosstalk between the neurons, (*ii*) providing metabolic supply to the neurons and thereby preventing neuronal degeneration/death (17, 19), and (*iii*) preventing aberrant neuronal connectivity by guiding secondary axon tract growth, pathfinding, and fasciculation during development (55).

Materials and Methods

Fly Stocks. The fly stocks were obtained from the Bloomington *Drosophila* Stock Center and the *Drosophila* Genetic Resource Center, Kyoto as descried in *SI Appendix*.

Molecular Cloning of Transgenic Rescue and Targeting Constructs. The V5-tagged CPES genomic rescue construct was generated using recombineering methods as described (56, 57). The UAS-GFP-GPI construct was made as described previously (58). The CPES-knockout line (*cpes*) was generated by ends-out homologous recombination (59) as detailed in *SI Appendix*.

Sphingolipidomics. Sphingolipids are estimated as described in *SI Appendix* and based on published protocols (31, 60, 61).

Development and Survival Analysis, Longevity, Photosensitive Epilepsy Experiments, Cortex Glial Counting, Western Analysis, and Transmission Electron Micrography. These experiments were performed as described in *SI Appendix*.

Calcium Imaging. Two-photon calcium imaging from freely behaving head-fixed *Drosophila* was performed as described previously (13). Details are provided in *SI Appendix*.

Immunohistochemistry. *Drosophila* tissues were dissected and immunostained as described previously (62–65). Details are provided in *SI Appendix*.

TLC for Sphingolipids. Lipids were extracted from 10 fly heads and were separated for sphingolipids on TLC as described previously (66). Details are provided in *SI Appendix*.

Metabolic Labeling and TLC Analysis of Phospholipids. Lipid extracts of *Drosophila* were analyzed for phospholipids by TLC using the method described previously (67). Details are provided in *SI Appendix*.

Metabolomics Analysis. The global metabolomics profile was determined for wild-type and *cpes* mutant flies (Dataset S3). Four biological replicates, each with 100 whole flies, were snap-frozen in liquid nitrogen, stored at −80 °C, and submitted to Metabolon, Inc. for GC-MS and LC-MS/MS analysis of metabolites.

Plasma Membrane Isolation. Plasma membrane was isolated essentially as described previously (68) with a few modifications as described in *SI Appendix*.

DRM Isolation. DRMs were isolated essentially as described previously (39) with a few modifications as described in *SI Appendix*.

ACKNOWLEDGMENTS. We thank Vivek Jayaraman for suggesting the experiments on calcium imaging in *Drosophila cpes* mutants and for providing the expertise and resources for performing the experiments in his laboratory (the Jayaraman laboratory is funded by the Howard Hughes Medical Institute); Dr. Manzoor Bhat for the contactin antibody; and Drs. Shyam Sharan, Ira Daar, Susan Mackem, Mark Lewandoski, and Terry Yamaguchi for comments on the manuscript. This study was funded by the Intramural Division of the National Cancer Institute, NIH, Department of Health and Human Services. U.A. is supported by NIH Grant RO1GM110288. The content of this publication does not necessarily reflect the views or policies of the Department of Health and Human Services, nor does mention of trade names, commercial products, or organizations imply endorsement by the US government.

1. Devinsky O, Vezzani A, Najjar S, De Lanerolle NC, Rogawski MA (2013) Glia and epilepsy: Excitability and inflammation. *Trends Neurosci* 36:174–184.
2. Poleon S, Szaflarski JP (2017) Photosensitivity in generalized epilepsies. *Epilepsy Behav* 68:225–233.
3. Fisher RS, Harding G, Erba G, Barkley GL, Wilkins A; Epilepsy Foundation of America Working Group (2005) Photic- and pattern-induced seizures: A review for the Epilepsy Foundation of America Working Group. *Epilepsia* 46:1426–1441.
4. Harding GF (1998) TV can be bad for your health. *Nat Med* 4:265–267.
5. Covanis A (2005) Photosensitivity in idiopathic generalized epilepsies. *Epilepsia* 46: 67–72.
6. Hermes D, Kasteleijn-Nolst Trenité DGA, Winawer J (2017) Gamma oscillations and photosensitive epilepsy. *Curr Biol* 27:R336–R338.
7. Kremer MC, Jung C, Batelli S, Rubin GM, Gaul U (2017) The glia of the adult Drosophila nervous system. *Glia* 65:606–638.
8. Awasaki T, Lai SL, Ito K, Lee T (2008) Organization and postembryonic development of glial cells in the adult central brain of Drosophila. *J Neurosci* 28:13742–13753.
9. Pereanu W, Shy D, Hartenstein V (2005) Morphogenesis and proliferation of the larval brain glia in Drosophila. *Dev Biol* 283:191–203.
10. Vacaru AM, van den Dikkenberg J, Ternes P, Holthuis JC (2013) Ceramide phosphoethanolamine biosynthesis in Drosophila is mediated by a unique ethanolamine phosphotransferase in the Golgi lumen. *J Biol Chem* 288:11520–11530.
11. Parker L, Padilla M, Du Y, Dong K, Tanouye MA (2011) Drosophila as a model for epilepsy: Bss is a gain-of-function mutation in the para sodium channel gene that leads to seizures. *Genetics* 187:523–534.
12. Bloomquist BT, et al. (1988) Isolation of a putative phospholipase C gene of Drosophila, norpA, and its role in phototransduction. *Cell* 54:723–733.
13. Seelig JD, et al. (2010) Two-photon calcium imaging from head-fixed Drosophila during optomotor walking behavior. *Nat Methods* 7:535–540.
14. Grienberger C, Konnerth A (2012) Imaging calcium in neurons. *Neuron* 73:862–885.
15. Chen TW, et al. (2013) Ultrasensitive fluorescent proteins for imaging neuronal activity. *Nature* 499:295–300.
16. Ghosh A, et al. (2013) A global in vivo Drosophila RNAi screen identifies a key role of ceramide phosphoethanolamine for glial ensheathment of axons. *PLoS Genet* 9: e1003980.
17. Stork T, Bernardos R, Freeman MR (2012) Analysis of glial cell development and function in Drosophila. *Cold Spring Harb Protoc* 2012:1–17.

18. Coutinho-Budd JC, Sheehan AE, Freeman MR (2017) The secreted neurotrophin Spätzle 3 promotes glial morphogenesis and supports neuronal survival and function. *Genes Dev* 31:2023–2038.
19. Spéder P, Brand AH (2018) Systemic and local cues drive neural stem cell niche remodelling during neurogenesis in *Drosophila*. *eLife* 7:e30413.
20. Rietveld A, Neutz S, Simons K, Eaton S (1999) Association of sterol- and glycosylphosphatidylinositol-linked proteins with Drosophila raft lipid microdomains. *J Biol Chem* 274:12049–12054.
21. Tafesse FG, et al. (2007) Both sphingomyelin synthases SMS1 and SMS2 are required for sphingomyelin homeostasis and growth in human HeLa cells. *J Biol Chem* 282: 17537–17547.
22. Ternes P, Brouwers JF, van den Dikkenberg J, Holthuis JC (2009) Sphingomyelin synthase SMS2 displays dual activity as ceramide phosphoethanolamine synthase. *J Lipid Res* 50:2270–2277.
23. Kunduri G, et al. (2014) Phosphatidic acid phospholipase A1 mediates ER-Golgi transit of a family of G protein-coupled receptors. *J Cell Biol* 206:79–95.
24. Kol M, et al. (2017) Switching head group selectivity in mammalian sphingolipid biosynthesis by active-site-engineering of sphingomyelin synthases. *J Lipid Res* 58: 962–973.
25. Subathra M, Qureshi A, Luberto C (2011) Sphingomyelin synthases regulate protein trafficking and secretion. *PLoS One* 6:e23644.
26. Tafesse FG, et al. (2013) Intact sphingomyelin biosynthetic pathway is essential for intracellular transport of influenza virus glycoproteins. *Proc Natl Acad Sci USA* 110: 6406–6411.
27. Deng Y, Rivera-Molina FE, Toomre DK, Burd CG (2016) Sphingomyelin is sorted at the trans Golgi network into a distinct class of secretory vesicle. *Proc Natl Acad Sci USA* 113:6677–6682.
28. Brand AH, Manoukian AS, Perrimon N (1994) Ectopic expression in Drosophila. *Methods Cell Biol* 44:635–654.
29. Subbaiah PV, Subramanian VS, Wang K (1999) Novel physiological function of sphingomyelin in plasma. Inhibition of lipid peroxidation in low density lipoproteins. *J Biol Chem* 274:36409–36414.
30. Sargis RM, Subbaiah PV (2006) Protection of membrane cholesterol by sphingomyelin against free radical-mediated oxidation. *Free Radic Biol Med* 40:2092–2102.
31. Rao RP, et al. (2007) Ceramide transfer protein function is essential for normal oxidative stress response and lifespan. *Proc Natl Acad Sci USA* 104:11364–11369.
32. Klapisz E, Masliah J, Béréziat G, Wolf C, Koumanov KS (2000) Sphingolipids and cholesterol modulate membrane susceptibility to cytosolic phospholipase A(2). *J Lipid Res* 41:1680–1688.
33. Nakamura H, et al. (2015) Sphingomyelin regulates the activity of secretory phospholipase A2 in the plasma membrane. *J Cell Biochem* 116:1898–1907.
34. Simons K, Toomre D (2000) Lipid rafts and signal transduction. *Nat Rev Mol Cell Biol* 1: 31–39.
35. Brown DA, London E (1998) Functions of lipid rafts in biological membranes. *Annu Rev Cell Dev Biol* 14:111–136.
36. Schroeder R, London E, Brown D (1994) Interactions between saturated acyl chains confer detergent resistance on lipids and glycosylphosphatidylinositol (GPI)-anchored proteins: GPI-anchored proteins in liposomes and cells show similar behavior. *Proc Natl Acad Sci USA* 91:12130–12134.
37. Mollinedo F, Gajate C (2015) Lipid rafts as major platforms for signaling regulation in cancer. *Adv Biol Regul* 57:130–146.
38. Gielen E, et al. (2006) Rafts in oligodendrocytes: Evidence and structure-function relationship. *Glia* 54:499–512.
39. Lingwood D, Simons K (2007) Detergent resistance as a tool in membrane research. *Nat Protoc* 2:2159–2165.
40. Faivre-Sarrailh C, et al. (2004) Drosophila contactin, a homolog of vertebrate contactin, is required for septate junction organization and paracellular barrier function. *Development* 131:4931–4942.
41. Fabini G, Freilinger A, Altmann F, Wilson IB (2001) Identification of core alpha 1,3-fucosylated glycans and cloning of the requisite fucosyltransferase cDNA from Drosophila melanogaster. Potential basis of the neural anti-horseadish peroxidase epitope. *J Biol Chem* 276:28058–28067.
42. Wolf P, Goosses R (1986) Relation of photosensitivity to epileptic syndromes. *J Neurol Neurosurg Psychiatry* 49:1386–1391.
43. Song J, Tanouye MA (2008) From bench to drug: Human seizure modeling using Drosophila. *Prog Neurobiol* 84:182–191.
44. Freeman MR (2010) Specification and morphogenesis of astrocytes. *Science* 330: 774–778.
45. Freeman MR, Doherty J (2006) Glial cell biology in Drosophila and vertebrates. *Trends Neurosci* 29:82–90.
46. Coulter DA, Steinhäuser C (2015) Role of astrocytes in epilepsy. *Cold Spring Harb Perspect Med* 5:a022434.
47. Slotte JP (2013) Biological functions of sphingomyelins. *Prog Lipid Res* 52:424–437.
48. Jin ZX, et al. (2008) Impaired TCR signaling through dysfunction of lipid rafts in sphingomyelin synthase 1 (SMS1)-knockdown T cells. *Int Immunol* 20:1427–1437.
49. Lafont E, et al. (2010) Caspase-mediated inhibition of sphingomyelin synthesis is involved in FasL-triggered cell death. *Cell Death Differ* 17:642–654.
50. Asano S, et al. (2012) Regulation of cell migration by sphingomyelin synthases: Sphingomyelin in lipid rafts decreases responsiveness to signaling by the CXCL12/CXCR4 pathway. *Mol Cell Biol* 32:3242–3252.
51. Dong L, et al. (2012) CD4+ T-cell dysfunctions through the impaired lipid rafts ameliorate concanavalin A-induced hepatitis in sphingomyelin synthase 1-knockout mice. *Int Immunol* 24:327–337.
52. Olsen ASB, Færgeman NJ (2017) Sphingolipids: Membrane microdomains in brain development, function and neurological diseases. *Open Biol* 7:170069.
53. Bromfield EB, Cavazos JE, Sirven J (2006) *An Introduction to Epilepsy* (American Epilepsy Society, West Hartford, CT).
54. Melom JE, Littleton JT (2013) Mutation of a NCKX eliminates glial microdomain calcium oscillations and enhances seizure susceptibility. *J Neurosci* 33:1169–1178.
55. Spindler SR, Ortiz I, Fung S, Takashima S, Hartenstein V (2009) Drosophila cortex and neuropile glia influence secondary axon tract growth, pathfinding, and fasciculation in the developing larval brain. *Dev Biol* 334:355–368.
56. Warming S, Costantino N, Court DL, Jenkins NA, Copeland NG (2005) Simple and highly efficient BAC recombineering using galK selection. *Nucleic Acids Res* 33:e36.
57. Venken KJ, He Y, Hoskins RA, Bellen HJ (2006) P[acman]: A BAC transgenic platform for targeted insertion of large DNA fragments in D. melanogaster. *Science* 314: 1747–1751.
58. Greco V, Hannus M, Eaton S (2001) Argosomes: A potential vehicle for the spread of morphogens through epithelia. *Cell* 106:633–645.
59. Gong WJ, Golic KG (2003) Ends-out, or replacement, gene targeting in Drosophila. *Proc Natl Acad Sci USA* 100:2556–2561.
60. Fyrst H, Herr DR, Harris GL, Saba JD (2004) Characterization of free endogenous C14 and C16 sphingoid bases from Drosophila melanogaster. *J Lipid Res* 45:54–62.
61. Merrill AH, Jr, Sullards MC, Allegood JC, Kelly S, Wang E (2005) Sphingolipidomics: High-throughput, structure-specific, and quantitative analysis of sphingolipids by liquid chromatography tandem mass spectrometry. *Methods* 36:207–224.
62. Zamore PD, Ma S (2011) Isolation of Drosophila melanogaster testes. *J Vis Exp* 2641.
63. Müller HA (2008) Immunolabeling of embryos. *Methods Mol Biol* 420:207–218.
64. Hafer N, Schedl P (2006) Dissection of larval CNS in Drosophila melanogaster. *J Vis Exp* 85.
65. Williamson WR, Hiesinger PR (2010) Preparation of developing and adult Drosophila brains and retinae for live imaging. *J Vis Exp* 1936.
66. Rao RP, et al. (2014) Ceramide transfer protein deficiency compromises organelle function and leads to senescence in primary cells. *PLoS One* 9:e92142.
67. Parthibane V, Rajakumari S, Venkateshwari V, Iyappan R, Rajasekharan R (2012) Oleosin is bifunctional enzyme that has both monoacylglycerol acyltransferase and phospholipase activities. *J Biol Chem* 287:1946–1954.
68. Papoulas O, Hays TS, Sisson JC (2005) The golgin Lava lamp mediates dynein-based Golgi movements during Drosophila cellularization. *Nat Cell Biol* 7:612–618.